

## On strong ground motion synthesis with $k^{-2}$ slip distributions

František Gallovič\* & Johana Brokešová

*Department of Geophysics, Faculty of Mathematics and Physics, Charles University, V Holešovičkách 2, Prague 8, 180 00, Czech Republic; \*Author for correspondence: tel: +420221912535, fax: +420221912555, e-mail: gallovic@karel.troja.mff.cuni.cz*

Received 12 November 2002; accepted in revised form 19 January 2004

*Key words:* heterogeneous slip distribution, kinematic source modelling, strong ground motions,  $\omega$ -squared model

### Abstract

This study deals with the methodical aspects of  $k^{-2}$  (Bernard et al., 1996) kinematic strong motions modelling: (1) it is shown how to incorporate the  $k$ -dependent rise time for 2D fault geometry in the strong motion synthesis according to the representation theorem, (2) it is suggested how to produce realistic  $k^{-2}$  slip models including asperity(ies), (3) modifications are introduced concerning the type of used slip velocity function and the corner wave number in the slip distribution. High frequency effects of these generalized models are discussed. It is shown that, assuming the rise time proportional to the spatial slip wavelength at high wave numbers, the spectral decay of displacement at frequencies higher than the corner frequency is given just by the decay of the slip distribution spectrum, regardless of the type of slip velocity function. It is shown numerically that this model provides  $\omega$ -squared source spectrum even in a vicinity of a 2D normal fault buried in 1D structure, which is an agreement with previous studies.

### Introduction

Modelling realistic time histories of displacement, velocity and acceleration in the vicinity of a fault is of great importance for seismic engineers in determining the structural response and in damage estimation. Especially, high-frequency accelerations are responsible for damage of common buildings with resonance frequencies higher than 1 Hz. In this respect, strong motion synthesis for moderate to large earthquakes needs a realistic source model in order to predict reliable time histories. In this paper, we are concerned with the kinematic modelling of the seismic source, not with rupture dynamics. We want to propose a realistic kinematic process on a finite-extent fault which would provide the desired  $\omega$ -squared source spectrum (Aki, 1967). We start from the  $k^{-2}$  rupture model, introduced by Bernard and Herrero (1994). The authors propose a kinematic self-similar random slip distribution with  $k^{-2}$  decay of amplitudes at high wave numbers  $k$ . They showed that rupture propagating unilaterally at constant velocity with such final

slip distribution, together with the instantaneous slip (i.e. the slip velocity function is  $\delta$ -pulse), radiates an  $\omega$ -squared source spectrum. If a more realistic slip velocity function is used, e.g., a box car, it acts as a low-pass filter, thus producing an undesired  $\omega$ -cubed source spectrum. To preserve the  $\omega$ -squared source spectrum, Bernard et al. (1996) proposed the boxcar with a  $k$ -dependent width (rise time).

The  $k^{-2}$  rupture model has already been successfully used for past as well as future earthquakes (e.g. Berge-Thierry et al., 2001; Zollo et al., 1997; Emolo and Zollo, 2001). All these papers emphasize the importance of considering complex source processes for estimating strong ground motion in the near-source region.

The aim of this paper is to discuss the methodological aspects of  $k^{-2}$  kinematic modelling of strong ground motions. We show how to incorporate the  $k$ -dependent rise time into the strong motion synthesis according to representation theorem for a 2D fault geometry in general media. We discuss some important attributes of the model (e.g., slip velocity function,

corner wave number in the slip distribution) and their consequences on the radiated spectra, especially, as regards directivity. We provide some suggestions how to produce realistic  $k^{-2}$  slip distributions including asperity(-ies). We numerically show that the model provides  $\omega$ -squared source spectrum in a vicinity of a 2D normal fault buried in 1D structure.

### Rectangular fault

We derive a general equation for strong motion synthesis for a kinematic 2D rectangular fault model with a wave number dependent rise time. In the frequency domain, acceleration  $\ddot{\mathbf{u}}$  measured at point  $\mathbf{r}$ , caused by a pure shear rupture, is given by the representation theorem (see, e.g., Aki and Richards, 1980)

$$\ddot{\mathbf{u}}(\mathbf{r}, f) = \iint_{\Sigma} d\xi \dot{\mathbf{H}}(\mathbf{r}, f; \xi) \Delta \dot{\mathbf{u}}(\xi, f). \quad (1)$$

where  $\mathbf{H}$  is the impulse response of the medium (obtained by, e.g. discrete wavenumber, finite difference, ray methods, etc.) and dots above the letter indicates the time derivative,  $\xi$  denotes the position on fault  $\Sigma$  and  $\Delta \dot{\mathbf{u}}$  is the time history of the slip velocity. Let us assume that any point on the fault follows slip rate history  $\Delta \dot{\mathbf{u}}_0(\xi, t)$  (starting at  $t = 0$ ) shifted in time as the rupture front expands. Denoting the rupture time  $t_r$ , in frequency domain we have

$$\Delta \dot{\mathbf{u}}(\xi, f) = \Delta \dot{\mathbf{u}}_0(\xi, f) e^{-2\pi i f t_r(\xi)}. \quad (2)$$

We express  $\Delta \dot{\mathbf{u}}_0$  in (2) using its inverse spatial Fourier transform. Inserting it in (1) we yield

$$\ddot{\mathbf{u}}(\mathbf{r}, f) = \iint_{\Sigma} d\xi \dot{\mathbf{H}}(\mathbf{r}, f; \xi) e^{-2\pi i f t_r(\xi)} \iint d\mathbf{k} \Delta \dot{\mathbf{u}}_0(\mathbf{k}, f) e^{2\pi i \mathbf{k} \cdot \xi}. \quad (3)$$

We assume that in the wave number domain,  $\Delta \dot{\mathbf{u}}(\mathbf{k}, f)$  can be factorized into product  $D(\mathbf{k})U(\mathbf{k}, f)$ , where  $D(\mathbf{k})$  represents the final slip for the given  $\mathbf{k}$  and  $U(\mathbf{k}, f)$  is the spectrum of the slip velocity function corresponding to unit final slip. Its duration in the time domain represents the rise time.

To take into account the wave number dependent rise time, we define function  $F(t)$  corresponding to the unit final dislocation with one second duration. The time scaling of  $U$  can then be expressed as  $U(\mathbf{k}, t) = F(t/\tau(\mathbf{k}))/\tau(\mathbf{k})$ . The unit final dislocation is

preserved by factor  $1/\tau(\mathbf{k})$ . In the frequency domain,  $U(\mathbf{k}, f) = X(f\tau(\mathbf{k}))$ , where  $X(f)$  is the Fourier spectrum of  $F(t)$ . Inserting it into Eq. (3) we obtain the representation theorem for a kinematic model with  $k$ -dependent rise time:

$$\ddot{\mathbf{u}}(\mathbf{r}, f) = \iint_{\Sigma} d\xi \dot{\mathbf{H}}(\mathbf{r}, f; \xi) e^{-2\pi i f t_r(\xi)} \iint d\mathbf{k} D X(f\tau(\mathbf{k})) e^{2\pi i \mathbf{k} \cdot \xi}. \quad (4)$$

The  $k$ -dependent rise time, slip and rupture time distributions for a 2D fault should be specified in such a way to preserve the main features proposed by Bernard and Herrero (1994) and Bernard et al. (1996) for a 1D (line) fault, namely to preserve the radiation of  $\omega$ -squared source spectra. In this way, the  $k^{-2}$  rupture model for a line fault (introduced in the above-mentioned studies) is extended to include the 2D fault geometry.

One of the basic assumptions of Bernard and Herrero (1994) is that the rupture propagates unilaterally at constant velocity  $v$ . For a 2D fault, we can assume the rupture to propagate radially at a constant velocity. The radial rupture propagation has been already taken into account by, e.g., Berge et al. (1998) and Hisada (2001).

Concerning the rise time variations, Bernard et al. (1996) suggested that the rupture propagates in the form of a slip pulse of dimension  $L_0$  (related to the maximum rise time by  $\tau_{max} = L_0/v$ ). Slip inhomogeneities of shorter characteristic dimensions rupture in time proportional to their spatial wavelength. The observational evidence for such pulses propagating over the fault are given by Heaton (1990).

More specifically, Bernard et al. (1996) introduced two parameters to quantify the relation between the rise time and the wave number. 1)  $\tau_{max}$  which controls the maximum duration of slip, and 2) a nondimensional coefficient  $a$  which controls, for a given slip wavelength  $\lambda$ , the ratio between the rise time and the time the rupture needs to cover distance  $\lambda$ . The authors suggested  $a = 0.5$ , which is also used in this paper. For the 2D fault geometry, we propose the rise time to be dependent on  $k = |\mathbf{k}|$  in the following way:

$$\tau(k) = \frac{\tau_{max}}{\sqrt{1 + \left(\frac{L_0 k}{a}\right)^2}}. \quad (5)$$

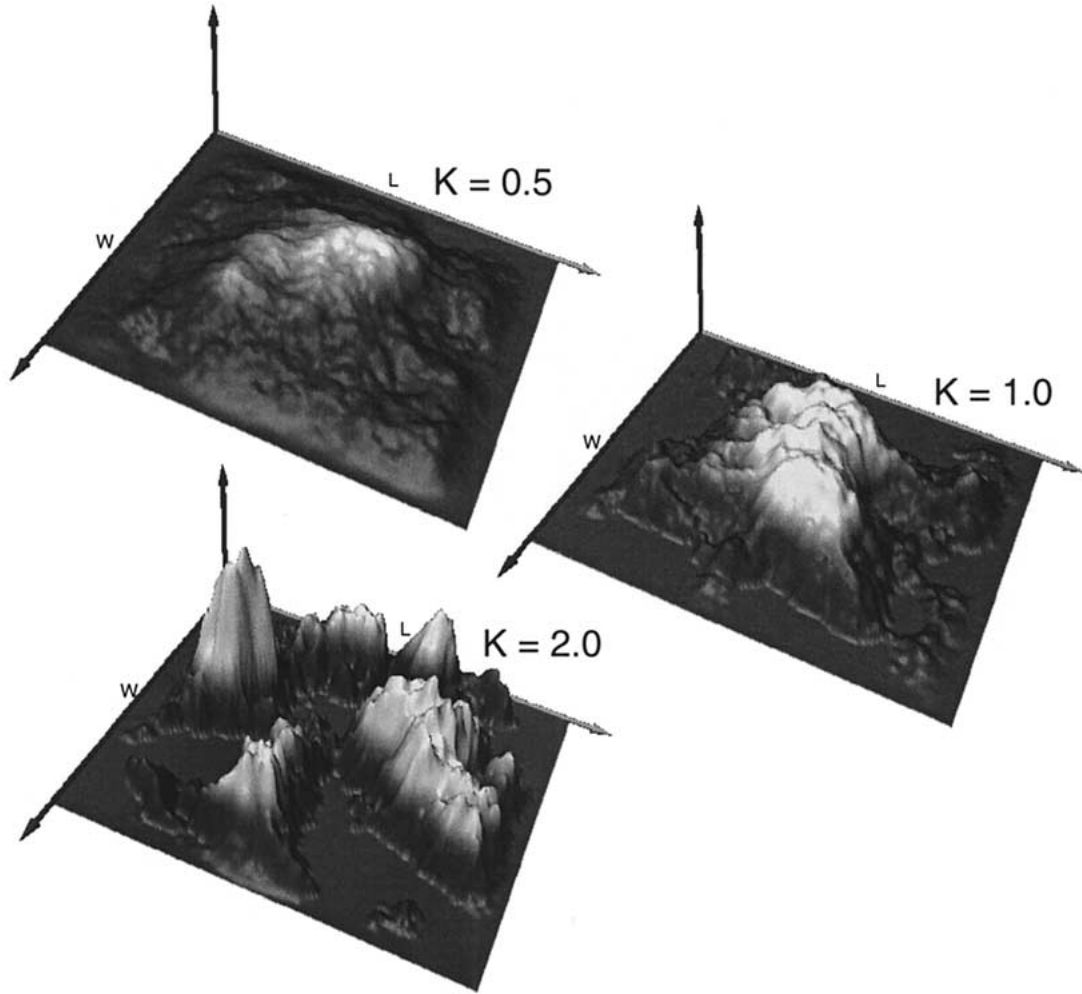


Figure 1. Three  $k^{-2}$  slip distributions for different values of  $K$  – the parameter controlling the corner wave number in (6). The mean slip is the same for all these cases.

### Slip distribution

According to Herrero and Bernard (1994) the  $k^{-2}$  asymptotic decay of the slip amplitude spectrum takes place beyond the corner wave number  $k_c = 1/L$ , where  $L$  is the characteristic dimension of the fault, while below the corner wave number the slip is independent of  $k$ . We investigate source models with a generalized corner wave number for the 2D fault of length  $L$  and width  $W$ , preserving the  $k^{-2}$  spectral decay.

We use the spatial 2D Fourier spectrum of the slip distribution in the following form

$$D(k_x, k_z) = \frac{\Delta \bar{u} L W}{\sqrt{1 + \left( \left( \frac{k_x L}{K} \right)^2 + \left( \frac{k_z W}{K} \right)^2 \right)^2}} e^{i\Phi(k_x, k_z)}, \quad (6)$$

where  $\Delta \bar{u}$  denotes the mean slip and  $\Phi$  is the phase spectrum. The terms  $L/K$  and  $W/K$  represent the correlation lengths of distribution (6) and their reciprocals are the corner wave numbers. Similar formula has been suggested by Somerville et al. (1999) and Hisada (2001). In Eq. (6)  $K$  is a dimensionless constant which controls the corner wave numbers and, consequently, the slip distribution ( $K$  plays similar role as  $a$  does in Eq. (5)).

Note that there are no restrictions on the phase spectrum of (6). According to Bernard and Herrero

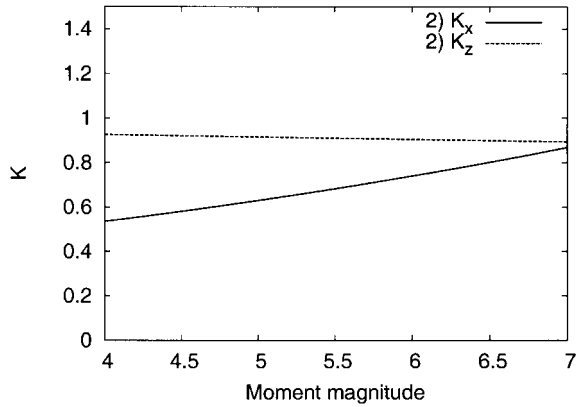


Figure 2. Empirical dependence of  $K$  on moment magnitude  $M_w$  after Somerville et al. (1999).  $K_x$  and  $K_z$  denote  $K$  in the strike and dip direction, respectively. Note that the paper prefer  $K < 1$  (corresponding to a relatively smooth slip).

(1994),  $\Phi$  is considered random at any wave number, except the circle  $k^2 = k_x^2 + k_z^2 \leq (1/L)^2 + (1/W)^2$  for which the phase is chosen so that the final slip is concentrated in the centre of the rectangular fault. This also means that we have no other physical constraints on the dislocation than the dimension of the fault and the mean slip. That is why we refer to this as the *random slip*. Examples of the random slip for various values of  $K$  are shown in Figure 1.

Let us discuss the corner wave numbers in slip distribution (6) in more detail. They have been already studied in papers dealing with source scaling relations (Somerville et al., 1999; Mai and Beroza, 2000; Mai and Beroza, 2001) where information about the correlation lengths (i.e.  $L/K$  or  $W/K$  in our notation) is extracted from smoothed slip inversion results, i.e. from data of relatively low resolution. (For tests of the slip inversion accuracy, see Graves and Wald, 2001, and Wald and Graves, 2001). Up to now no more than about tens of slip models have been examined for magnitudes in the range about  $5 < M_w < 8$  (see [http://www-socal.wr.usgs.gov/wald/slip\\_models.html](http://www-socal.wr.usgs.gov/wald/slip_models.html) for available slip models of the western North America earthquakes). An empirical curve according to Somerville et al. (1999) showing the magnitude scaling of  $K$  (determined from the empirical relations for the corner wave numbers and rupture dimensions derived in the paper) are in Figure 2. It can be seen that the empirical relations suggest  $K < 1$ . However, it should be taken into account that the values in Figure 2 are rather underestimated due to the smooth character of the slip derived from the inversions. On the other hand, there is evidence supporting

the small value of  $K$ : the  $K = 2$  case in Figure 1 shows quite large areas of zero slip which is not supported by the slip inversions (Bernard, personal communication). These considerations led us to choose  $K = 1$ . (Note that, e.g., 20% variations of  $K$  around 1 cannot be excluded).

Note that considering a random slip with  $K = 1$  means one slip patch in the center of the fault (see Figure 1). Such concentration of the seismic moment (slip) at the centre of the fault is probably not very realistic for whole range of magnitudes. It may be valid for small earthquakes, perhaps asperities, but not for moderate to large ruptures in general for which the slip inversions indicate occurrence of two or more asperities on the fault at various positions.

>From the above discussion it follows that we need to generate slip models consisting of asperities, but with  $K$  around 1 retaining the  $k^{-2}$  spectral decay at high wave numbers. Such slip models can be obtained by introducing the so-called *hybrid slip* generator (originally proposed by Hisada, 2001, for the slip inversion results). We consider the deterministic part of the final slip on long scales. It can be obtained, for example, from slip inversions, from some empirical relations, or from some tectonic properties of the region. Alternatively, in the strong motion prediction studies the asperity position can be subjected to variations. The stochastic part of the slip is then superimposed on the remaining scales.

An example of the hybrid slip distribution containing one asperity can be found in Figure 3. The procedure to generate the hybrid slip can consist of four steps:

- Layout of the blocks of constant slip with the dimension of  $\Delta L \times \Delta W$  representing the deterministic part of the slip (left side of Figure 3).
- Smoothing.
- Transforming to the wave number domain.
- Prescribing the  $k^{-2}$  spectral decay by applying function (6) with random phase for  $k > k_N$ , where  $k_N$  is Nyquist's wave number of the deterministic part ( $k_N^2 = (1/\Delta L)^2 + (1/\Delta W)^2$ ). In this way, we in fact add some 'noise' to the deterministic part of the slip distribution.

The smoothing of the dislocation (second step) is necessary to avoid spectral holes caused by the sharp edges of the layout blocks<sup>1</sup>. We use simple smoothing

<sup>1</sup> The amplitude spectrum of a box corresponds to function  $\text{sinc}(f)$ . This oscillatory function reaches zero for some values of  $f$ . Such spectral holes are an artefact of the unphysical assumption that the deterministic part of the slip consists of blocks.

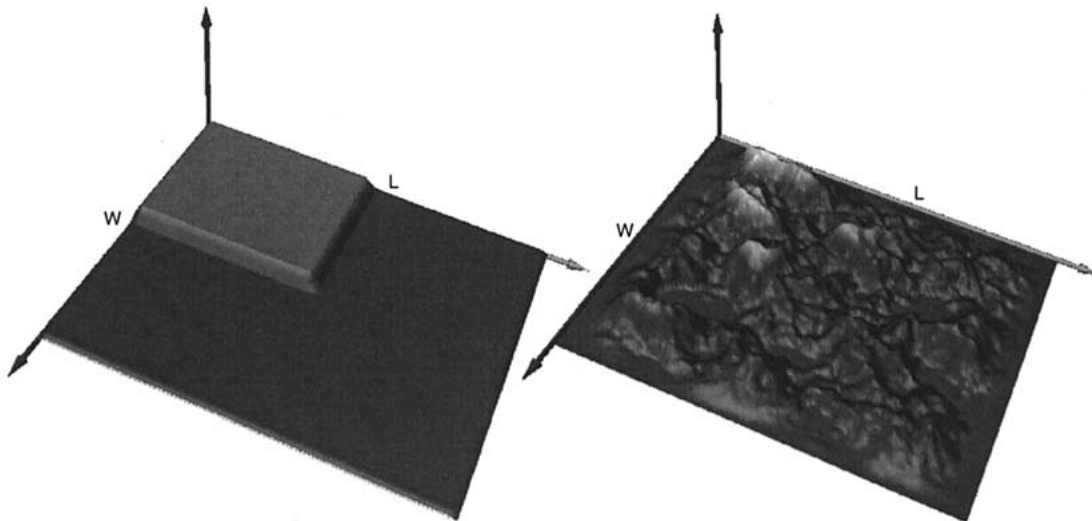


Figure 3. An example of the hybrid slip model with one asperity. Left: the deterministic part of the slip distribution. Right: the resulting hybrid slip.

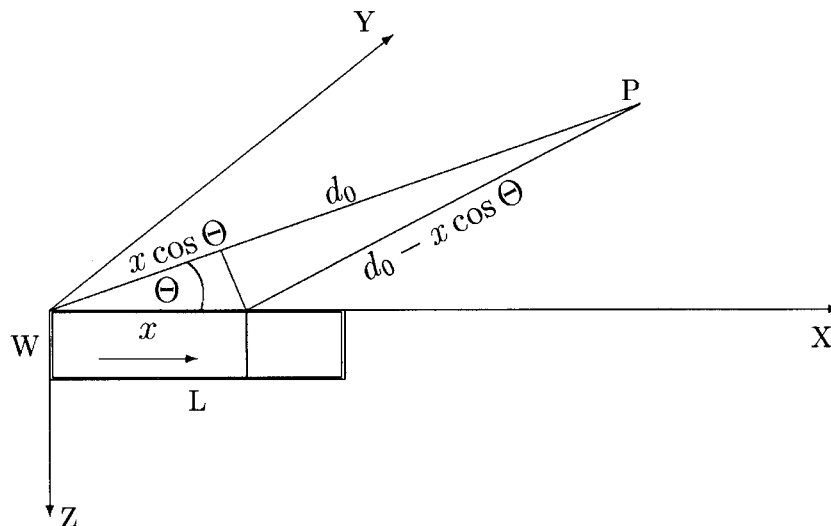


Figure 4. The geometry used for the line fault approximation with unilateral rupture propagation. The coordinate system is connected with the fault. The rupture propagates in the  $x$  direction.

with a sliding window.

The hybrid slip generator (Fortran code) is freely available from the authors.

### The influence of $k^{-2}$ model parameters

To understand the influence of the source model parameters on the radiated wave field, it is suitable to

express source time functions analytically. The corresponding formulae can be obtained under the following, commonly used, simplifying assumptions: a line fault in Fraunhofer's approximation with unilateral rupture propagation in homogeneous space (see Figure 4). The amplitude factor representing the radiation pattern is assumed to be constant with respect to the position on the fault. It can be shown (see Appendix in this paper, or Gallovič, 2002) that the representation

theorem then simplifies to the form

$$\ddot{u}(f) = (2\pi if)^2 C D(k'_x, k'_z) X(f\tau(k'_x, k'_z)),$$

$$k'_z = \frac{f}{vC_d}, k'_x = 0 \quad (7)$$

with

$$C = \frac{\mu F^c}{4\pi\rho c^3 d_0} e^{-i2\pi f d_0/c},$$

where  $\mu$  is the rigidity,  $\rho$  the density,  $F^c$  is a value given by the radiation pattern, and  $d_0$  is the epicentral distance.  $C_d$  is the directivity coefficient dependent on the angle from fault strike  $\Theta$  (see Figure 4) and on ratio  $v/c$  between rupture velocity  $v$  and wave propagation velocity  $c$ :

$$C_d = \frac{1}{1 - (v/c) \cos \Theta}. \quad (8)$$

After inserting (5) and (6) into (7) we obtain the following expression for the amplitude spectrum:

$$|\ddot{u}(f)| = (2\pi f)^2 \frac{\mu F^c}{4\pi\rho c^3 d_0} \frac{\Delta\bar{u}LW}{\sqrt{1 + \left(\frac{fL}{vC_d K}\right)^4}}$$

$$\left| X \left( f \sqrt{\frac{\tau_{max}}{1 + \left(\frac{fL_0}{vC_d a}\right)^2}} \right) \right|. \quad (9)$$

Let us briefly discuss the shape of such amplitude spectrum following the discussion for the case of box-car slip velocity function ( $X(f) = \text{sinc}(f)$ ) by Bernard et al. (1996). To recognize the directivity effects better, we consider isotropic radiation pattern ( $F^c$  not depending on  $\Theta$ ).

First, let us examine the special case of the instantaneous slip ( $X(f) = 1$ ). Eq. (9) then simplifies to

$$|\ddot{u}(f)| = (2\pi f)^2 \frac{\mu F^c}{4\pi\rho c^3 d_0} \frac{\Delta\bar{u}LW}{\sqrt{1 + \left(\frac{fL}{vC_d K}\right)^4}}. \quad (10)$$

Comparing (10) and (6) we can see that the displacement spectrum  $u(f)$  at a given frequency would correspond to the wave number spectrum of slip distribution  $D$  at wave number  $k'_x = \frac{f}{vC_d}$  (while  $k'_z = 0$ ). Consequently, the spectral decay of the apparent source time function corresponds to the spectral decay of the dislocation distribution for  $k_z = 0$ .

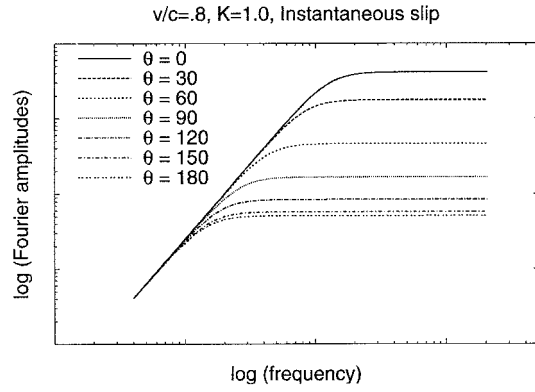


Figure 5. The apparent acceleration source spectra radiated by the  $k^{-2}$  rupture model with instantaneous slip for various values of  $\Theta$ . Note the angular dependence of the apparent corner frequency and the spectral plateau.

The above-mentioned assumptions for slip distribution  $D$  yield a rupture model providing an  $\omega$ -squared source spectrum. Examples of the apparent acceleration source spectra for various angles  $\Theta$  can be seen in Figure 5. Notice that the apparent corner frequency,

$$f_a = \frac{vC_d K}{L}, \quad (11)$$

is controlled by the corner wave number in dislocation distribution (6). It is not affected by the fault length itself but by the correlation length  $L/K$  and  $C_d$ , i.e.  $f_a$  varies with the angle relative to the fault (directivity effect).

Figure 5 also shows another effect of directivity: the angular variation of the height of the acceleration plateau. It can be examined, for any slip velocity function, using Eq. (9):

$$|\ddot{u}(f \rightarrow \infty)| = \frac{\pi F^c M_0}{\rho c^3 d_0} f_a^2 X(aC_d), \quad (12)$$

where  $M_0 = \mu\Delta\bar{u}LW$  is the scalar seismic moment.

Especially for the instantaneous slip, the height of the acceleration plateau is proportional to  $C_d^2$  (due to proportionality to  $f_a^2$ ), which has been firstly concluded by Joyner (1991). It represents a very strong directivity effect. For  $v/c = 0.9$ ,  $C_d^2$  would reach 100 in the direction of rupture propagation. Such high frequency amplification has not been observed (Bernard et al., 1996). Note that such strong directivity effect is due to the instantaneous slip assumption. If a more realistic slip velocity function (of non-zero duration) is considered, the directivity effect becomes less pro-

nounced: the angular dependence of the acceleration plateau decreases by a factor of  $X(aC_d)$ . This results in more realistic accelerograms in the direction of rupture propagation.

It follows from Eq. (9) that the source spectrum has another corner frequency. This is called the *transition frequency*

$$f_0 = \frac{vC_d a}{L_0}. \quad (13)$$

The transition frequency was firstly expressed by Bernard et al. (1996). The transition frequency is connected with the corner wave number of rise time distribution (5). It is influenced by the width of the propagating slip pulse  $L_0$  and by  $C_d$ . The effect of  $f_0$  on the source spectra is discussed later.

Since in this study we concentrate on the methodical aspects of the kinematic source modeling, we consider useful to examine several standardly used slip velocity functions. The first one is a boxcar (used by Bernard et al., 1996) function, which is hardly acceptable from the point of view of source dynamics. The second one is more realistic Kostrov-like function proposed by Hisada (2000). The third one is Brune's function, which can be easily expressed as

$$F(t) = \begin{cases} f_b^2 t e^{-f_b t}, & t \geq 0 \\ 0, & t < 0 \end{cases}, \quad (14)$$

where parameter  $f_b$  controls the effective width of Brune's function. One of the most important advantages is its smoothness (in principle it could qualitatively understood as a smoothed version of the Hisada's pulse).

All discussed functions and then amplitude spectra are shown in Figure 6. The amplitude spectrum of Boxcar function exhibit undesirable spectral holes, while the amplitude spectra of Hisada's and Brune's functions are smooth. The spectral decays of boxcar's and Hisada's function are very similar to each other in the frequency region of our interest, while the Brune's function amplitude spectrum falls off faster.

The acceleration amplitude spectra for the boxcar, Brune's and Hisada's slip velocity functions for two widths of the propagating pulse are displayed in Figure 7. As we can see, the acceleration levels for Hisada's and Brune's slip rate functions are higher than that for the boxcar function. However, they are lower compared with the instantaneous slip case (Figure 5). To better illustrate this, we show the amplification at high frequencies in Figure 8. By the amplification term we understand quantity  $C_d^2 X(aC_d)$  see Eq. (12).

As regards the direction of rupture propagation, the assumption of the instantaneous slip would generate strong acceleration pulses. On the other hand, the use of the boxcar slip rate function results in underestimated pulses when compared with pulses provided by the more realistic Brune's and Hisada's slip velocity functions.

Let us discuss the acceleration spectra in the frequency range between the apparent corner and transition frequencies (see Figure 9 for illustration). Similar discussion can be found in paper by Bernard et al. (1996) but for special case of boxcar slip velocity function only. Note that  $f_a < f_0$  since  $K/L < aL_0$  (see (11) and (13)). At low frequencies ( $f < f_a$ ),  $\ddot{u}(f) \propto f^2 X(f\tau_{max})$ . Since at low frequencies  $X(f)$  is nearly constant (see Figure 6),  $\ddot{u}(f)$  behaves similarly to the impulsive slip rate function. This means that  $\ddot{u}(f)$  is not affected by the finite duration of the slip rate function, i.e the spectral amplification proportional to  $C_d^2$  (see the model with instantaneous rise time) is preserved. Between  $f_a$  and  $f_0$  (middle frequencies), the slip velocity function of finite duration starts to act as a low-pass filter because  $X(f)$  starts to decay (Figure 6). However, behind the transition frequency (high frequencies), the terms in brackets under both square roots are  $\gg 1$  (so that 1 can be neglected). Consequently,  $\ddot{u}(f)$  does not depend on  $f$ . To summarize, the  $k^{-1}$  proportionality of the rise time causes the source acceleration spectrum to be independent of frequency, i.e. we obtain a plateau at high frequencies. Thus, although this model can be understood as consistent with the observed  $\omega$ -squared model, it prescribes the more complicated behaviour at middle frequencies.

Note that, regardless of the station position, the  $K$ -parameter (originating from the corner wave number of the dislocation distribution) affects the source spectrum: the corner frequency and the height of the acceleration spectral plateau are proportional to  $K$  and  $K^2$ , respectively. Note that it does not affect the source spectrum at low frequencies (seismic moment).

### An example: 1999 Athens earthquake

Up to now we have studied the influence of the model parameters in the farfield of linear fault in homogeneous medium. However, the model is capable to consider a 2D rectangular fault in a general medium (see Eq. (4)). A parametric study on PGA maps for such general case is presented by Gallovič and

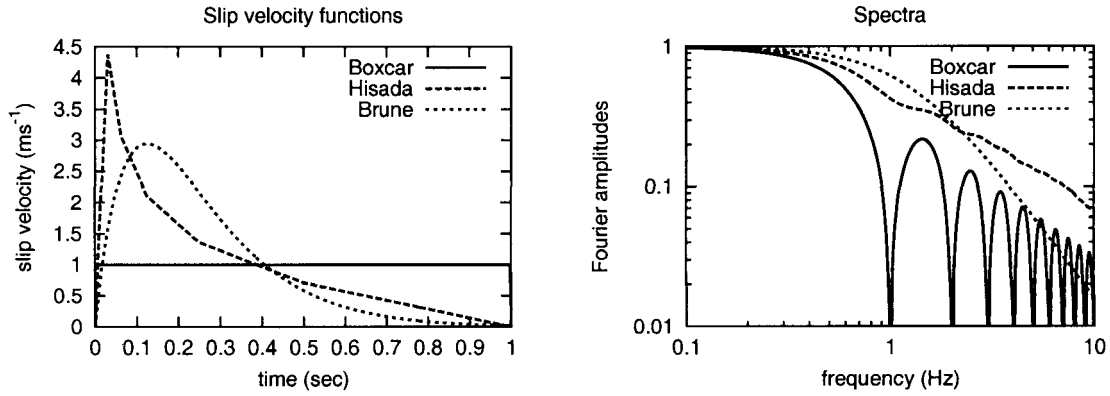


Figure 6. Three slip velocity functions (left) used in this study with their amplitude spectra (right). Hisada's function is constructed according to Hisada (2000) for a special choice of parameters describing the function:  $N_V = 5$  and  $f_{max} = 16s^{-1}$ . Brune's function is computed according to (14) with  $f_b = 8s^{-1}$ . All three functions have 1 sec duration and correspond to unit finite dislocation ( $f_b$  was chosen in such a way that the Brune's function reaches at 1 sec about 1/1000 of its maximum).

Brokešová (submitted). We show here just an example of the strong motion synthesis in 1D layered medium for a normal fault, based on model of the 1999 Athens earthquake ( $M_w = 5.9$ ), to demonstrate that the model provides  $\omega$ -squared source spectrum even in the near source distances where the assumptions made in previous sections (linear fault, Fraunhofer's approximation, homogeneous space) are violated.

Table 1. Fixed parameters for the Athens earthquake model

Lat. (N)	38.08°
Long. (E)	23.58°
Hypocentral depth [km]	12.0
Moment [Nm]	$7.8 \cdot 10^{17}$
Strike	123°
Dip	55°
Rake	-84°
Rupture velocity [km/s]	2.8

As regards the source model, we adopt the magnitude, location, depth, focal mechanism and the fault orientation from previous studies (for review see Zahradník, 2002). The parameters are listed in Table 1. The remaining parameters needed for the  $k^{-2}$  model ( $L$ ,  $W$ ,  $L_0$  etc.) are obtained from the empirical relations of Somerville et al. (1999) (see Table 2).

Somerville et al. (1999) suggested 1 or 2 asperities for the magnitude we are concerned with. For simplicity, we use the hybrid slip consisting of only 1 asperity with the mean slip twice larger than the mean slip over the whole fault. A sample realization

Table 2. Fixed parameters for the Athens earthquake model obtained from the empirical relations of Somerville et al. (1999). The maximum rise time  $\tau_{max}$  is determined to be twice longer than the average rise time yielded by the corresponding scaling relation

$L$ [km]	11
$W$ [km]	8
mean slip [m]	0.27
$\tau_{max}$ [sec]	0.84
$L_0$ [km]	2.35
Area of fault covered by asperity	0.25
Average asperity slip contrast	2.0

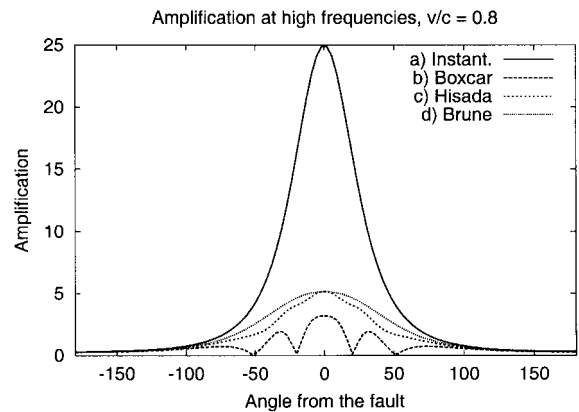


Figure 8. Azimuthal dependence of directivity amplification  $C_d^2 X(aCd)$  (height of the accelerogram spectral plateau, see Eq. (12)) at high frequencies for the slip velocity functions studied in this text. Note the relatively strong/weak amplification for the instantaneous/boxcar case with respect to Brune's and Hisada's case. The oscillatory character of the amplification in the boxcar case is a consequence of its unrealistic shape.

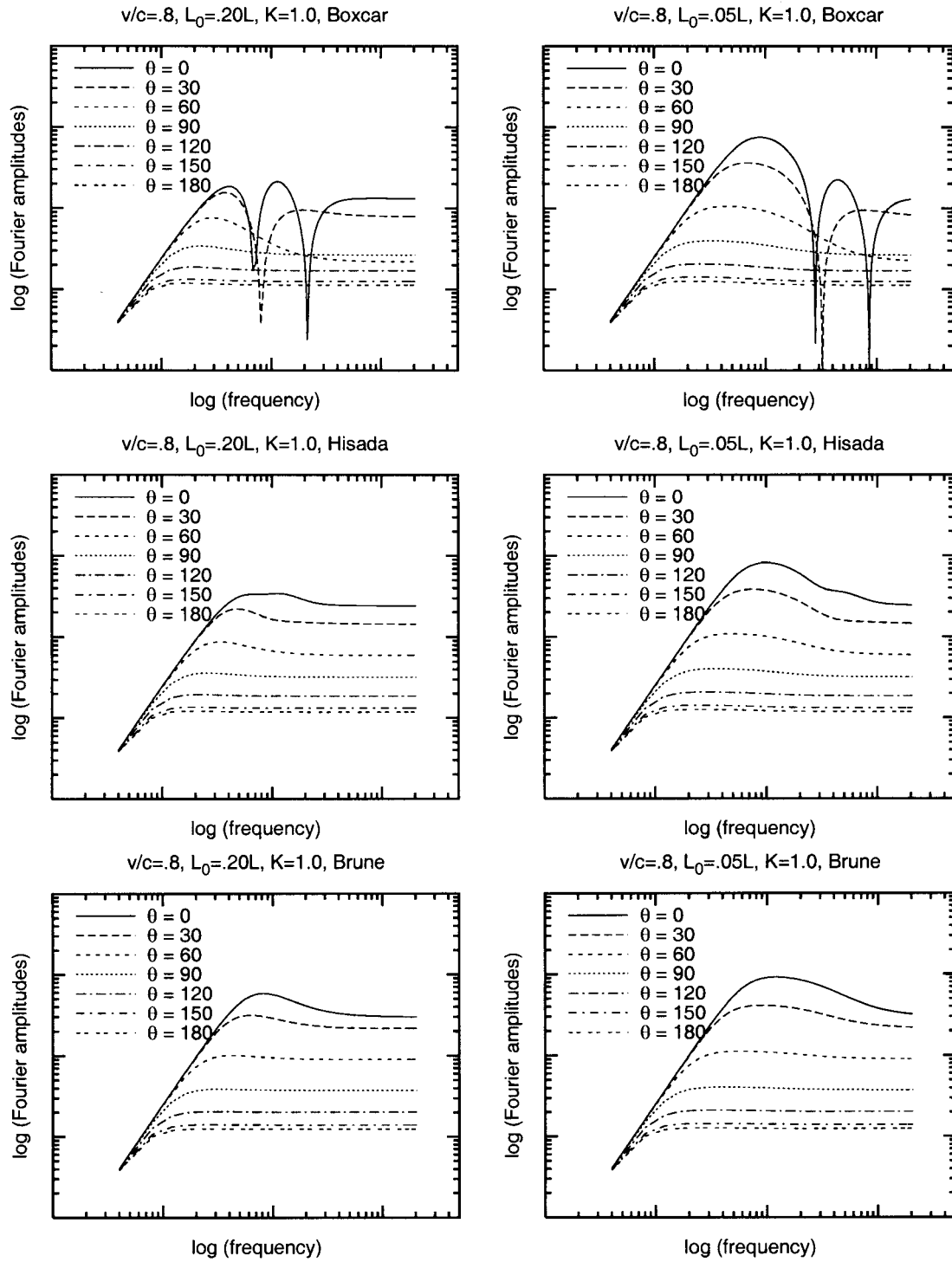


Figure 7. Acceleration amplitude spectra in the case of the wave number dependent rise time with two different slip pulse widths (columns) and three different slip velocity functions (rows). The boxcar case is modified from Bernard et al. (1996). The ranges of axes are the same as in Figure 5.

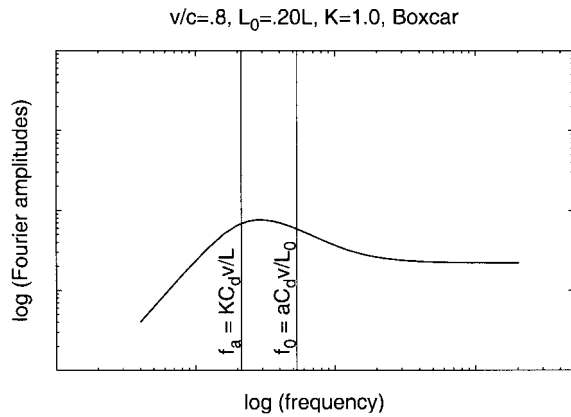


Figure 9. Acceleration amplitude spectrum taken from the top left panel of Figure 7 for  $\Theta = 60^\circ$ . The apparent ( $f_a$ ) and transition ( $f_0$ ) corner frequencies of the model are displayed. The ranges of axes are the same as in Figure 5 and 7.

of the hybrid slip distribution used is displayed in Figure 3. To pronounce the directivity effect, we assume according to Plicka and Zahradník (2002) that the nucleation point (corresponding to the hypocentre) is located in the bottom left corner of the asperity. The rupture propagates radially at a constant rupture velocity. Hisada's slip velocity function is assumed.

The 1D crustal model, originally used for discrete wave number modelling of regional Athens earthquake data by Tselentis and Zahradník (2000) (model MA), was chosen for our computations. This model is partially supported in the paper by Novotný et al. (2001).

Since we are interested in the source time functions and their spectra, we compute direct S-wave only by means of the ray method (we could also consider P-wave only but the S-wave is more eligible in strong motion studies) and we neglect the attenuation and site effects. The computer code for 2D ray computations BEAM87, written by Červený and modified by Brokešová (1993) (see also Opršal et al., 2002), to allow for 2.5D computations is used. By the 2.5D computation we understand the computation of 3D rays in a 2D medium (i.e. a medium with properties depending on the vertical and one horizontal coordinate, in general)<sup>2</sup>. In our case, however, the model is 1D only, so that at this stage we do not utilize the full advantage of the 2.5D approach mentioned above

<sup>2</sup> Note that in the seismological literature the term '2.5D modelling' is often understood in a much less general sense (calculation of 2D in-plane rays while considering point source radiation, see, e.g., Bleistein, 1984; Lafond and Levander, 1990).

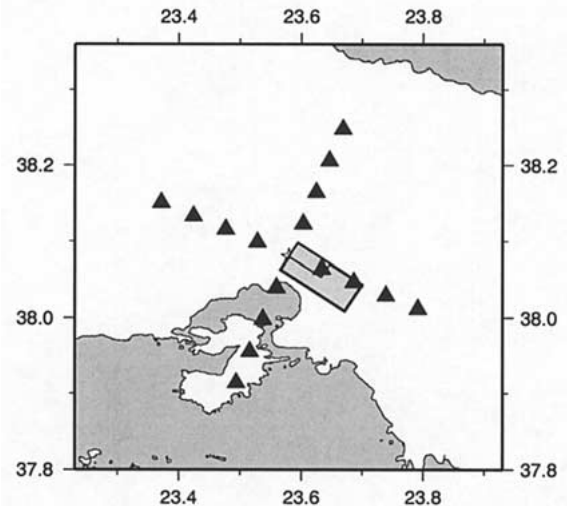


Figure 10. The geometry for the synthetic example. The rectangles in the middle of the map represent the projection of the fault and the asperity onto the earth's surface (see also Figure 3). The star denotes the epicentre and the triangles the stations.

(our rays are only plane curves). The extension to 2D models in future would be straightforward.

The receivers are distributed radially around the epicenter in four perpendicular directions. In each direction, there are 4 receivers at epicentral distances of 5 to 20 km at steps of 5 km. The geometry is shown in Figure 10.

The rays for each receiver are traced from grid points distributed sparsely on the fault ( $20 \times 15$ ), and then the parameters of the ray solution (travel times and complex amplitudes) are interpolated by bicubic splines into a grid dense enough to evaluate the representation integral ( $128 \times 64$ ). The interpolation enables significantly faster computation of the synthetics (e.g., Brokešová, 1996; Berge-Thierry, 2001). Note that in the ray approach it is not necessary to interpolate Green's functions as a whole, but it is sufficient to interpolate only the ray solution parameters which, in this particular model, exhibit relatively smooth behaviour with respect to the spatial coordinates on the fault.

The synthesis is performed according to Eq. (4) up to 5Hz, which is above the apparent corner frequency. The accelerograms and their spectra (obtained for a single slip realization) are shown in Figure 11. The figure contains four panels corresponding to four epicentral distances under study. Within each panel we can compare the synthetics for four azimuths to study the directivity effects.

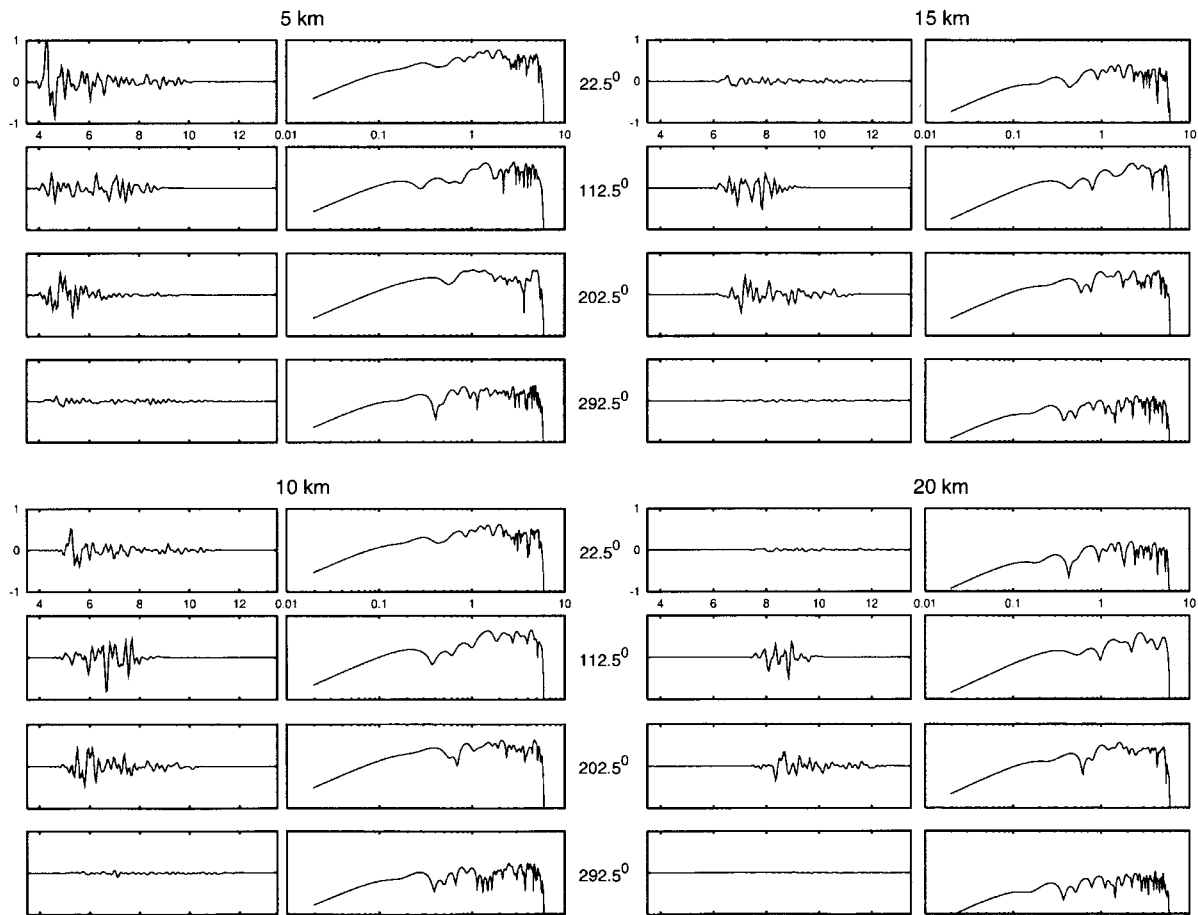


Figure 11. Synthetic accelerograms (in  $m/s^2$ ) and their amplitude spectra: the four panels correspond to four epicentral distances and four azimuths from the north clockwise. Note the directivity effects: the amplitude and duration of the accelerogram, the height of the accelerogram spectral plateau and the corner frequency vary significantly with the azimuth. The time scale is in seconds, the frequency scale in Hz.

In particular, stations of azimuth  $112.5^\circ$  lies in the direction of rupture propagation and, thus, the duration of the records is shorter and amplitudes are larger with respect to records at stations in the opposite direction (of azimuth  $292.5^\circ$ ). Synthetics at stations located to the south and north from the south-dipping fault exhibit different maximal amplitudes even if they lie in the same epicentral distances. The nearest station (5 km) to the north is affected by up-dip directivity combined with maximum in S-wave radiation pattern and, thus, its synthetic is the strongest. For more distant north stations both effects vanishes while the southern stations still lie in the direction of S-wave radiation pattern lobe, which causes that their amplitudes becomes larger than the amplitudes of northern stations at the same epicentral distances.

Generally, in spite of the near fault location of the receivers, the acceleration spectra exhibit the desired spectral plateau beyond the corner frequency. According to our tests, these features of the source functions are independent of the slip distribution realization. This validates the 2D extension of the  $k^{-2}$  rupture model, which is in agreement with previous studies dealing with this kinematic model (e.g. Berge-Thierrg et al., 2001; Zollo et al., 1997; Emolo and Zollo, 2001).

## Discussion and conclusion

The paper concentrates on the methodical aspects of strong ground motion synthesis based on the  $k^{-2}$  rupture model of Bernard et al. (1996). The approach developed here allows for general models, however in

the presented example (1999 Athens earthquake) we do not utilize the full advantage of the presented approach since we did not have a more complex model at our disposal.

Let us summarize the most important methodical aspects of our approach:

1. We propose a simple analytical expression (4) for kinematic strong motion synthesis for a 2D fault model buried in general medium, including the wave number dependent rise time (Bernard et al., 1996). For faster computations in the far-field approximation with a general slip velocity function, the instantaneous rise time can be used, while the spectral plateau is then corrected according to Eq. (9) (Beige-Thierry et al., 2001).
2. In order to generalize the  $k^{-2}$  slip model, the corner wave number  $K/L$  ( $L$  being the fault length) in the  $k^{-2}$  stochastic slip distribution of Bernard and Herrero (1994) has been discussed. It has been shown that the  $K$ -parameter controls the smoothness/roughness of the slip distribution. We discussed current indirect observations (inverted slip models) and conclude that the preferred value of  $K$  is around 1. To model realistic slip distributions with  $K = 1$  consisting of asperities we suggest an easy way to generate so-called hybrid slip (originally proposed by Hisada, 2001, for the slip inversion results). Note that in this paper single parameter  $K$  has been introduced for simplicity although, in general, there should be two parameters  $K_x$  and  $K_z$  controlling the corner wave number in strike and dip directions, respectively. This more strict approach (with both  $K_x$  and  $K_z$ ) will be studied in future.
3. To provide a flexible tool for simulating a variety of earthquakes, the restriction to a boxcar slip velocity function (with wave number dependent rise time) discussed in Bernard et al. (1996) was relaxed. It was found that the desired  $\omega$ -squared source spectrum can be generated by any slip velocity function whose rise time is proportional to the spatial slip wavelength at high wave numbers. Thus, the spectral decay at frequencies higher than the corner frequency is given only by the decay of the slip distribution spectrum, regardless of the type of slip velocity function. This shows that the  $\omega$ -squared source model is robust enough and could also explain why the  $\omega$ -squared decay is observed so commonly.
4. The theoretical study of the effect of various slip velocity functions on the ground acceleration has

shown that the instantaneous slip and the boxcar function represent the limiting cases. The instantaneous slip overestimates the accelerations while the boxcar underestimates them with respect to more general slip velocity functions (e.g., Brune's and Hisada's in this study). >From this point of view the case with instantaneous rise time can represent 'extreme' scenario for strong ground motion prediction (Zollo et al., 1997 and Emolo and Zollo, 2001). On the other hand, for modelling real data we suggest using any slip velocity function of non-zero duration (e.g., Brune's, Hisada's).

The  $k^{-2}$  rupture modelling with properties described in this paper has been applied to a general model of normal fault buried in a layered medium. This synthetic experiment has shown that the generalization of the  $k^{-2}$  model to 2D fault provides  $\omega$ -squared source spectrum even in short epicentral distances. This is in agreement with previous studies dealing with this kinematic model (e.g. Berge-Thierry et al., 2001; Zollo et al., 1997; Emolo and Zollo, 2001).

Available Fortran code: The hybrid slip generator is freely available from the authors.

## Appendix

Here we briefly show how to derive Eq. (7) from Eq. (4), i.e. how to get simple analytical formula for a line fault (in Fraunhofer's approximation with unilateral rupture propagation in homogeneous space) from representation theorem for 2D rupture model in general medium to (for geometry see Figure 4). For simplicity we consider magnitude of displacement  $u=|u|$  only.

The assumption of linearity of the fault simplifies formula (4) to

$$\ddot{u}(r, f) = \int_0^L dx \dot{H}(r, f; x) e^{-2\pi i f t_r(x)}$$

$$\int dk_x D(k_x, k'_z) X(f \tau(k_x, k'_z)) e^{2\pi i k_x x}, k'_z = 0 \quad (15)$$

Since slip distribution in the spatial domain  $D(x)$  is identically zero outside the fault (i.e. for  $x < 0$  and  $x > L$ ), the limits of the integral with respect to  $x$  in the formula (15) can be extended to infinity. In the following we omit writing the limits of the integral.

For homogeneous space, time derivative of the impulse response  $\dot{H}$  can be expressed as

$$\dot{H}(r, f; x) = (2\pi i f)^2 \frac{\mu F^c}{4\pi \rho c^3 d(r, x)} e^{-2\pi i f d(r, x)/c}, \quad (16)$$

where  $d(r, x)$  is the distance from source to receiver. The description of other quantities can be found in the text of this paper.

The rupture is assumed to propagate unilaterally along the  $x$ -axis at constant rupture velocity  $v$ , thus, we can express the rupture time as  $t_r(x) = x/v$ . Let us express distance  $d(r, x)$  in the Fraunhofer's approximation (valid only for observers situated far from the fault with respect to the length of the fault) as  $d \doteq d_0 - x \cos \Theta$ , where  $d_0$  is the hypocentral distance (see Figure 4). As far as the amplitude coefficient in Eq. (16) is considered, we assume that the variations of  $d$  and  $F^c$  with  $x$  are negligible compared to hypocentral distance  $d_0$ . Then, inserting (16) to (15) we get

$$\ddot{u}(r, f) = (2\pi i f)^2 C \int dx e^{-2\pi i f x / v C_d} \int dk_x D(k_x, k'_z) X(f \tau(k_x, k'_z)) e^{2\pi i k_x x}, k'_z = 0 \quad (17)$$

where  $C$  and  $C_d$  (directivity coefficient) are defined by (7) and (8), respectively.

Integrating (17) with respect to  $x$  we obtain

$$\ddot{u}(r, f) = (2\pi i f)^2 C \int dk_x D(k_x, k'_z) X(f \tau(k_x, k'_z)) \delta\left(k_x - \frac{f}{v C_d}\right), k'_z = 0 \quad (18)$$

>From this, integrating with respect to  $k_x$ , we come easily to Eq. (7).

## Acknowledgements

Suggestions and comments by Pascal Bernard greatly improved this paper. The authors are also very grateful to Jiří Zahradník and anonymous referees for helpful review and comments. Many thanks also belong to Kojiro Irikura for invaluable discussions. Some of the figures were made with Generic Mapping Tools (Wessel and Smith, 1991). The authors were supported by the following grants: EU project EVG1-CT-1999-00001 PRESAP and several research projects in the Czech Republic – MSM 113200004, GACR 205/03/1047 and GAUK 176/2000/B GEO/MFF.

## References

Abrahamson, N.A. and Shedlock, K., 1997, Overview, *Seis. Res. Letters* **68**, 9–23.  
 Aki, K., 1967, Scaling law of seismic spectrum, *J. Geophys. Res.* **72**, 1217–1231.

Aki, K. and Richards, P.G., 1980, *Quantitative Seismology: Theory and Methods*, W.H. Freeman, San Francisco.  
 Berge-Thierry, C., Bernard, P. and Herrero, A., 2001, Simulating strong ground motion with the ' $k^{-2}$ ' kinematic source model: An application to the seismic hazard in the Erzincan basin, Turkey, *J. Seismology* **5**, 85–101.  
 Bernard, P. and Herrero, A., 1994, Slip heterogeneity, body-wave spectra, and directivity of earthquake ruptures, *Annali di Geofisica* **XXXVII**, 1679–1690.  
 Bernard, P., Herrero, A. and Berge, C., 1996, Modeling directivity of heterogeneous earthquake ruptures, *Bull. Seism. Soc. Am.* **86**, 1149–1160.  
 Bleistein, N., 1984, *Two-and-one-half Dimensional In-Plane Wave Propagation*, Research report, Center of Wave Phenomena, Colorado School of Mines, Golden, Colorado.  
 Brokešová, J., 1993, *High-Frequency Ground Motions due to Extended Seismic Sources in Complex Structures*, PhD. Thesis, Charles University, Prague.  
 Brokešová, J., 1996, Construction of ray synthetic seismograms using interpolation of travel times and ray amplitudes, *PAGEOPH* **148**(3-4), 503–538.  
 Emolo, A. and Zollo, A., 2001, Accelerometric radiation simulation for the September 26, 1997 Umbria-Marche (Central Italy) main shocks, *Annali di Geofisica* **44**, 605–617.  
 Gallovič, F., 2002, *High Frequency Strong Motion Synthesis for  $k^{-2}$  Rupture Models*, Master Thesis, Charles University, Prague, <http://geo.mff.cuni.cz/students/gallovic>.  
 Gallovič, F. and Brokešová, J., 2002, The  $k^{-2}$  rupture model parametric study: example of the 1999 Athens earthquake, submitted to *Studia geoph. et geod.*  
 Graves, R. and Wald, D., 2001, Resolution analysis of finite fault source inversion using one- and three-dimensional Green's functions, 1. Strong motions, *J. Geophys. Res.* **106**, 8745–8766.  
 Hanks, T.C., 1982, fmax, *Bull. Seism. Soc. Am.* **72**, 1867–1879.  
 Heaton, T.H., 1990, Evidence for and implications of self-healing pulses of slip in earthquake rupture, *Phys. Earth Planet. Int.* **64**, 1–20.  
 Herrero, A. and Bernard, P., 1994, A kinematic self-similar rupture process for earthquakes, *Bull. Seism. Soc. Am.* **84**, 1216–1228.  
 Hisada, Y., 2000, A theoretical omega-square model considering the spatial variation in slip and rupture velocity, *Bull. Seism. Soc. Am.* **90**, 387–400.  
 Hisada, Y., 2001, A theoretical omega-square model considering the spatial variation in slip and rupture velocity. Part 2: Case for a two-dimensional source model, *Bull. Seism. Soc. Am.* **91**, 651–666.  
 Joyner, W., 1991, Directivity for non-uniform ruptures, *Bull. Seism. Soc. Am.* **81**, 1391–1395.  
 Lafond, C.F. and Levander, A.R., 1990, Fast and accurate dynamic raytracing in heterogeneous media, *Bull. Seism. Soc. Am.* **80**, 1284–1296.  
 Mai, M., and Beroza, C., 2000, Source scaling properties from finite-fault rupture models, *Bull. Seism. Soc. Am.* **90**, 604–615.  
 Mai, P.M. and Beroza, G.C., 2001, A spatial random-field model to characterize complexity in earthquake slip, *J. Geophys. Res.*, in review.  
 Novotný, O., Zahradník, J. and Tselentis, G.A., 2001, Northwestern Turkey earth-quakes and the crustal structure inferred from surface waves observed in western Greece, *Bull. Seism. Soc. Am.* **91**, 875–879.  
 Opršal, L., Brokešová, J., Faeh, D. and Giardini, D., 2002, 3D hybrid ray-FD and DWN-FD seismic modeling for simple models containing complex local structures, *Stud. Geophys. Geod.*, in press.

- Plicka, V. and Zahradník, J., 2002, Inversion of rupture nucleation from regional records by EGF method for unequal focal mechanisms of the mainshock and aftershock: The Athens 1999 earthquake, *Tectonophysics*, in press.
- Somerville, P., Irikura, K., Graves, R., Sawada, S., Wald, D., Abrahamson, N., Kagawa, Y.I.T., Smith, N. and Kowada, A., 1999, Characterizing crustal earthquake slip models for the prediction of strong ground motion, *Seis. Res. Lett.* **70**, 59–80.
- Tselentis, G.A. and Zahradník, J., 2000, The Athens earthquake of 7 September 1999, *Bull. Seism. Soc. Am.* **90**, 1143–1160.
- Wald, D. and Graves, R., 2001, Resolution analysis of finite fault source inversion using one- and three-dimensional Green's functions, 2. Combining seismic and geodetic data, *J. Geophys. Res.* **106**, 8767–8788.
- Wessel, P. and Smith, W.H.F., 1991, Free software helps map and display data, *EOS Trans. AGU* **72**, 441, 445–446.
- Zahradník, J., 2002, *Focal Mechanism of the Athens 1999 Earthquake by ASPO Method*, Res. Report, Dept. of Geophysics, Faculty of Math. and Phys., Charles University, Prague, <http://seis30.karlov.mff.cuni.cz>.
- Zahradník, J. and Tselentis, G.A., 2002, *Modeling Strong-Motion Accelerograms by 'PEXT' Method, Application to the Athens 1999 Earthquake*, Proc., European Seismological Commission (ESC); XXVIII General assembly, Genoa, Italy, September 1–6, CD-ROM.
- Zollo, A., Bobbio, A., Emolo, A., Herrero, A. and De Natale, G., 1997, Modeling of ground acceleration in the near source range: the Case of 1976, Friuli Earthquake (M=6.5), Northern Italy, *J. Seismol.* **1**, 305–319.